Laser-Assisted Reactivity of Triethylgallium or Trimethylgallium with Ammonia in Constrained Pulsed Nozzle Expansions

Alexander Demchuk, John Porter, and Brent Koplitz*

Department of Chemistry, Tulane University, New Orleans, Louisiana 70118

Received: July 23, 1998; In Final Form: September 9, 1998

The results of laser-assisted reactivity in constrained gas expansions involving either triethylgallium (TEGa) or trimethylgallium (TMGa) with ammonia are reported. NH_3 (or ND_3) along with TEGa or TMGa are introduced into a high vacuum chamber through a customized dual-source pulsed nozzle assembly. Excimer laser output (193 or 248 nm) is focused into the mixing and reaction region of the nozzle source, and a quadrupole mass spectrometer interrogates the photolyzed expansion. During gas mixing and expansion into the vacuum, the adduct signals from TMGa:NH_3 or TEGa:NH_3 are observed when the nozzle assembly is cooled. Laser irradiation of the gas mixtures results in the formation of new adducts, TMGa:NH_2 or TEGa:NH_2, and diverse, higher mass GaN-containing species. Power and wavelength dependence studies are used to reveal the photolytic origins of individual mass spectral features, and the influence of sample pressure on cluster formation processes is also examined.

I. Introduction

In recent years, metalorganic chemical vapor deposition (MOCVD) has been a widely used growth technique for fabricating III−V wide band-gap semiconductors, especially with regard to GaN and related materials having unique optoelectronic properties.[1−3] The MOCVD growth process for III−V materials is typically accomplished by the reaction of metal alkyls with hydrides of the nonmetal components. In GaN growth, trimethylgallium (TMGa) and ammonia (NH_3) are frequently used as precursors. The growth temperatures in these processes are often high (> 1000 °C) due to the need to pyrolyze the NH_3 precursor.[4] Even the decomposition of TMGa requires a moderately high temperature (∼370−500 °C).[5,6] However, high temperature in general is one of the disadvantages of the MOCVD growth technique and its ability to obtain sharp interface properties and minimize the generation of defects during thin film fabrication.[7]

In principle, lasers can be used to address the problem of requisite high temperatures in MOCVD growth by providing a lower temperature avenue by which precursor compounds can be "cracked." Although issues such as sufficient surface mobility may still require elevated temperatures, the chemical decomposition aspects of the MOCVD process can be addresssed, in part, by using lasers. In fact, pulsed lasers in combination with pulsed nozzle sources offer opportunities for significantly altering the chemical composition of the species that are finally delivered to a growth surface. Although actual film growth is not addressed experimentally in this paper, film growth studies are currently underway in our laboratory. In the present work, basic photoassisted reactivity and clustering is explored using a cooled nozzle extender assembly. Pioneered by Smalley and co-workers for cooling radicals and generating clusters from ablated targets,[8,9] the nozzle extender approach has been modified to allow for cooling as well as to incorporate two independently controlled nozzles, one for each precursor. The reaction length (and thereby the reaction time) for the mixture can be varied. Also, the reaction conditions with respect to temperature are affected by cooling the extender.

Early work by Chaiken and co-workers studied the photolytic production of metal clusters, specifically Pt, from an organometallic precursor.[10] In the current paper, we take advantage of the aforementioned cooled extender, which changes the composition of the expansion even in the absence of any laser radiation, and explore the constrained reactive photochemistry of TEGa as well as TMGa in combined expansions with NH_3. The net effect is a novel way to explore photoassisted cluster growth, where the precursors are standard metalorganic compounds commonly used to grow the desired semiconductor materials, in this case GaN. Not only can one make GaN-containing species, but the chemical pathways identified at these early growth stages may prove useful in understanding and ultimately optimizing laser-assisted macroscopic growth processes.

II. Experimental Section

The experimental apparatus has been described previously.[11] Briefly, it consists of a high vacuum chamber equipped with a quadrupole mass spectrometer (QMS) and a specialized dual pulsed nozzle source. A sample handling assembly (EMCORE Co.) allows one to control the backing pressure of the liquid metalorganic precursor by controlling its temperature. TEGa or TMGa (99+% purity, Strem Chemical) and NH_3 (99.99% purity, Air Products) are introduced into the high vacuum chamber via the nozzle assembly. TEGa and TMGa are used with He, Ar, or N_2 (99.9995% purity, Nova Gas) as the carrier gas. The vapor of TEGa or TMGa is fed into the sample chamber by passing the carrier gas through a temperature-controlled stainless steel bubbler. A pulse of each sample gas, either TMGa or TEGa and NH_3, is independently injected into the mixing/reaction region of the nozzle assembly (see Figure 1), which can be cooled to approximately 0 °C through the use of a coiled shroud of copper tubing. For the experimental results reported here, the TMGa and TEGa backing pressures were typically 200 Torr in 2000 Torr of carrier gas, while the NH_3

10.1021/jp983131j CCC: $15.00
Published on Web 10/21/1998

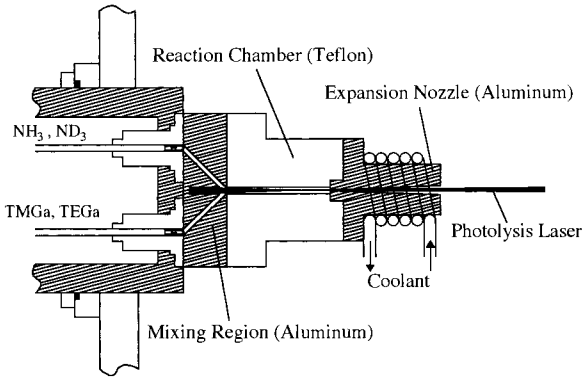

Figure 1. Schematic of dual pulsed-nozzle source.

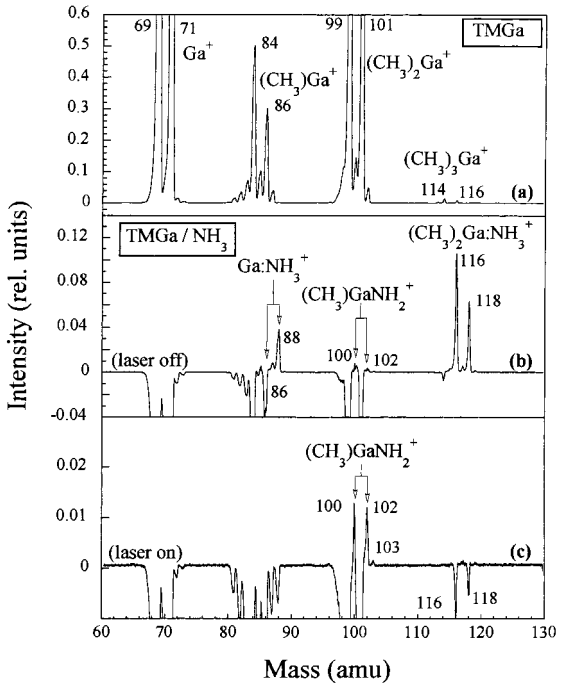

Figure 2. Low mass EI spectra observed using (a) TMGa alone, (b) $TMGa/NH_3$ without laser radiation, and (c) $TMGa/NH_3$ with laser radiation (193 nm, 5 mJ/pulse). For (b), the signal due to TMGa alone was subtracted, and for (c), the signal due to (b) was subtracted.

backing pressure was ~2200 Torr. However, the individual backing pressures were varied between 200 and 5000 Torr as needed in order to explore pressure effects on reactivity. The opening time of each pulsed valve was adjusted to be ~0.2−0.3 ms with repetition rates of 10 Hz. In some cases, ND_3 (99% D-atom purity, Cambridge Isotope Laboratory) was used instead of NH_3 in order to label the products and distinguish different reaction pathways.

To effect photoreactivity, the 193 or 248 nm output from an excimer laser (Lambda Physik LEXtra 200) is moderately focused with a quartz lens (focal length = 250 mm) into the mixing/reaction region of the nozzle through a 0.7 mm diameter hole. Laser beam energies ranging from 0.1 to 20 mJ/pulse were used, and the delay time between sample injection and laser pulse (typically ~5 ms) was adjusted to maximize product signal. However, the delay time between sample injection and laser pulse was also varied between 0 and 90 ms as needed in order to explore pressure effects in the nozzle source on cluster formation. The repetition rate of sample injection/laser irradiation is usually 10 Hz with 500 pulses being averaged. Reaction products are analyzed with a QMS (UTI 100C), and ion signals are recorded on a digital oscilloscope (LeCroy 9370).

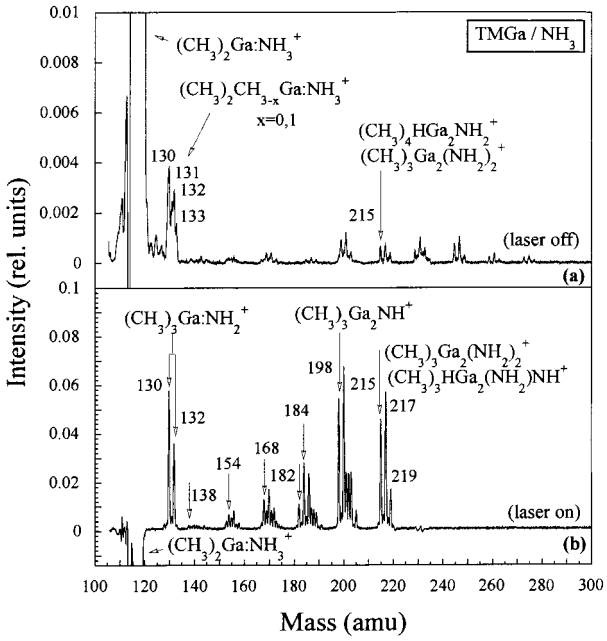

Figure 3. EI mass spectra of adduct and cluster products generated by the expansion of $TMGa/NH_3$ (a) without laser radiation and (b) with laser radiation (193 nm, 5 mJ/pulse). For (a), the signal due to TMGa alone was subtracted, and for (b), the signal due to (a) was subtracted.

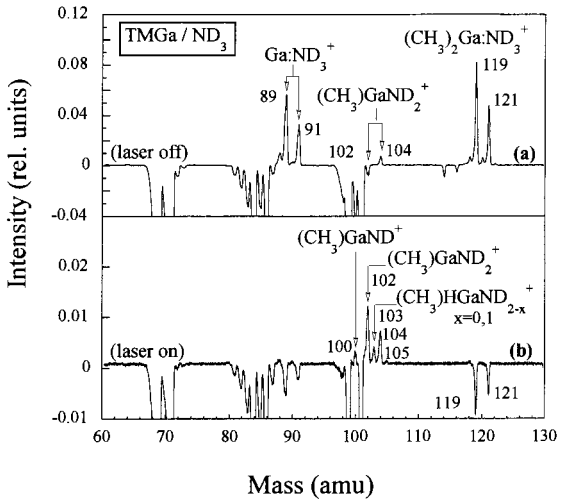

Figure 4. Low mass EI spectra observed using $TMGa/ND_3$ (a) without laser radiation and (b) with laser radiation (193 nm, 5 mJ/pulse). For (a), the signal due to TMGa alone was subtracted, and for (b), the signal due to (a) was subtracted.

III. Results and Discussion

When TMGa and NH_3 are combined, the main gas-phase reaction at low temperature is a strong Lewis acid/base interaction that results in production of a solid adduct compound $(CH_3)_3Ga{:}NH_3$.[12−16] When the adduct is heated above 90 °C, methane is eliminated and the trimer $[(CH_3)_2Ga{:}NH_2]_3$ is detected.[17,18] In our laboratory, we combine pulsed valves and a cooled nozzle extender to explore chemistry at conditions well below room temperature. Here, as discussed below, reactive chemistry involving these precursors is observed both with and without laser radiation.

A. Reactivity in the Absence of Photons. Figures 2−7 present the low and high mass regions of the 70 eV electron impact (EI) mass spectra observed during $TMGa/NH_3$ (or ND_3) and $TEGa/NH_3$ (or ND_3) expansions with the "laser off" and the "laser on." For reference, the EI mass spectrum of a neat

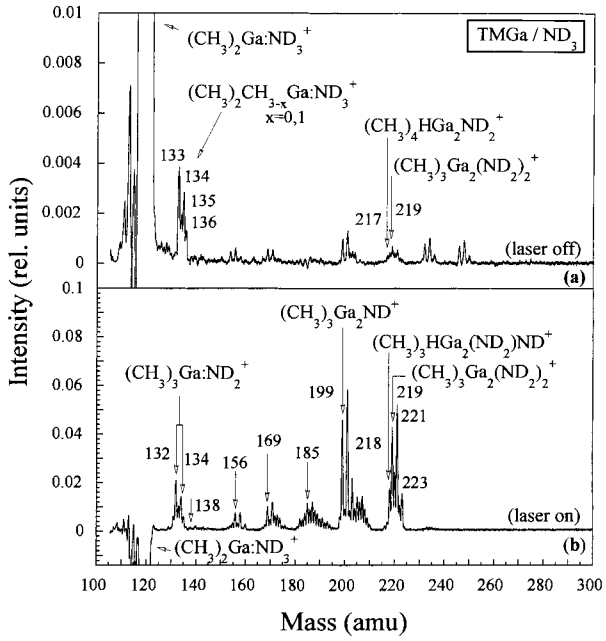

Figure 5. EI mass spectra of adduct and cluster products generated by the expansion of $TMGa/ND_3$ (a) without laser radiation and (b) with laser radiation (193 nm, 5 mJ/pulse). For (a), the signal due to TMGa alone was subtracted, and for (b), the signal due to (a) was subtracted.

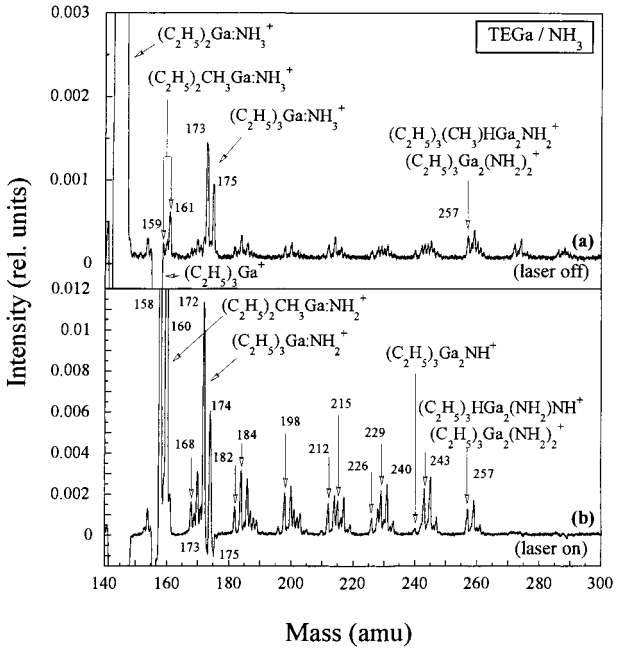

Figure 6. EI mass spectra of adduct and cluster products generated by the expansion of $TEGa/NH_3$ (a) without laser radiation and (b) with laser radiation (193 nm, 5 mJ/pulse). For (a), the signal due to TEGa alone was subtracted, and for (b), the signal due to (a) was subtracted.

TMGa expansion is presented in Figure 2a. Note that the expansion of TEGa alone (not shown) produces analogous features. When TMGa (or TEGa) is expanded with NH_3 (or ND_3), a Lewis acid/base adduct is formed and is clearly detected by the electron impact (EI) ionization technique when the cooled extender is used. Figures 2b and 3a present respectively portions of the low and high mass regions of the mass spectra that result when TMGa and NH_3 are combined in the dual nozzle assembly *in the absence of laser radiation*. These spectra are generated by subtracting the individual TMGa mass spectrum (Figure 2a) from the spectrum obtained when the two are mixed.

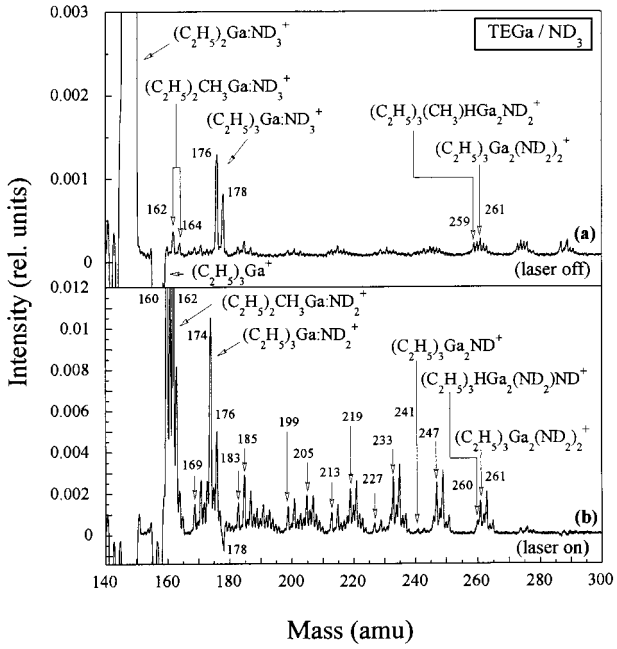

Figure 7. EI mass spectra of adduct and cluster products generated by the expansion of $TEGa/ND_3$ (a) without laser radiation and (b) with laser radiation (193 nm, 5 mJ/pulse). For (a), the signal due to TEGa alone was subtracted, and for (b), the signal due to (a) was subtracted.

During the mixing and expansion of TMGa and NH_3, a strong $(CH_3)_2Ga:NH_3$ ion signal is observed at 116/118 amu (Figure 2b) that displays the appropriate gallium isotope ratio. The relative abundance of the two isotopes of gallium is 60.4% and 39.6% for ^{71}Ga and ^{69}Ga, respectively.[19] Figure 3a shows the position of the parent adduct ion feature (masses 131/133) as well as those corresponding to the loss of an H-atom (masses 130/132). Here, the signal intensity has dropped by a factor of 25 for the parent adduct ion when compared with the $(CH_3)_2Ga:NH_3^+$ feature suggesting that significant fragmentation is occurring during the ionization process. Also, it should be added that we only observe the parent adduct signal when the nozzle extender is cooled.

To further identify fragmentation pathways, deuterated studies were conducted using ND_3. When $(CH_3)_3Ga$ and ND_3 are used, the $(CH_3)_2Ga:ND_3$ adduct ion feature with masses of 119/121 amu is clearly identified (Figure 4a). In addition, Figure 5a not only positively identifies a parent ion adduct feature, $(CH_3)_3Ga:ND_3^+$, in the mass range 133−136 amu, but it indicates that hydrogen loss comes primarily from the methyl, not the ammonia, part of the molecule. In Figure 5a, $(CH_3)_3Ga:ND_3^+$ has the same fragmentation pattern as the $(CH_3)_3Ga:NH_3^+$ region of Figure 3a, just shifted by 3 amu. If hydrogen loss were coming from the ammonia portion of the complex, this pattern would be altered upon switching to ND_3.

When TEGa and NH_3 are combined in the cooled nozzle assembly, the parent adduct signal $(C_2H_5)_3Ga:NH_3^+$ at 173/175 amu is observed, as shown in Figure 6a. Analogous to TMGa and NH_3, a very prominent feature is observed at 144/146 amu that corresponds to the loss of an alkyl group, in this case ethyl. Consistently, the $(C_2H_5)_3Ga:ND_3$ adduct at mass 176/178 amu and associated fragments, e.g., $(C_2H_5)_2Ga:ND_3$ at 147/149 amu, are detected when ND_3 is used in lieu of NH_3 (see Figure 7a). Finally, in the upper traces of Figures 3 and 4−7, one observes in the higher mass region evidence for small clustering (Figure 6a and Figure 7a). Analysis of these spectra show that both TMGa with NH_3 and TEGa with NH_3 produce analogous mass spectral features.

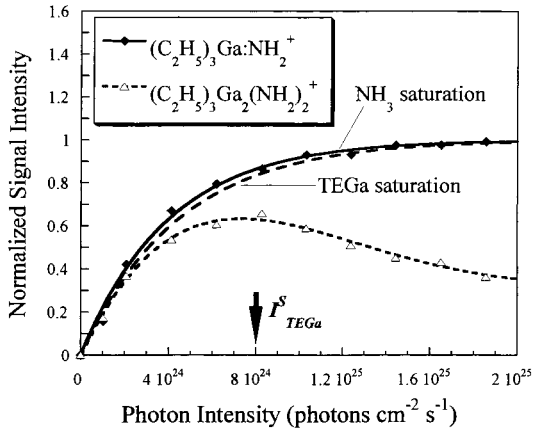

Figure 8. Normalized signal intensity of ion mass 172 amu, $(C_2H_5)_3Ga:NH_2$, and ion mass 257 amu, $(C_2H_5)_3Ga_2(NH_2)_2$, as a function of photon intensity. The photon intensity is calculated by fitting the $(C_2H_5)_3Ga:NH_2^+$ experimental data with eq 3 and the ammonia absorption cross section ($\sim 1 \times 10^{-17}$ cm^{-2}).

B. Laser-Initiated Reactivity. The lower traces in Figures 2−7 show the effects of introducing 193 nm laser radiation into the mixing/expansion region. Laser irradiation of the expanding mixture (either TMGa/NH_3 or TEGa/NH_3) results in photolysis of the precursor and adduct molecules as well as clustering effects. These spectra are generated by subtracting the mass spectra measured separately with and without laser radiation. Several qualitative observations are apparent. A comparison of the intensity scales reveals that signals for the higher mass peaks have increased by roughly an order of magnitude for the "laser on" data when compared with the "laser off" results. Depletion of the adduct features may be due to photon absorption by the adduct itself or a change in the formation pathway brought about by photolysis of a precursor species. Laser photolysis causes the $(CH_3)_3Ga$ (or $(C_2H_5)_3Ga$) molecules and the $(CH_3)_3Ga:NH_3$ (or $(C_2H_5)_3Ga:NH_3$) adduct molecules and their daughter fragment features to decrease significantly in intensity as evidenced by the negative peaks shown in these spectra.

Simultaneously, laser irradiation of these gas mixtures generates the rich, higher mass features shown in Figures 3b, 5b, 6b, and 7b. The chemical identities of these higher clusters are not certain. These spectra reveal a series of intense peaks that can be assigned to a mixture of products including R_3Ga_2NH, $R_3Ga_2(NH_2)_2$, and $R_3Ga_2(NH_3)NH$ ions along with their fragments, where R is a CH_3 or a C_2H_5 group. Less intense peaks can be attributed to $R_4Ga_2(NH_2)NH$ and $R_3HGa_2(NH_2)NH$ ions as well as the associated fragments.

C. Power and Wavelength Dependence Studies. Identification of the photolytic origins of individual mass features constitutes an avenue by which one can begin to explore the buildup of GaN-containing species. Clearly identified in the mass spectra are the $(CH_3)_3Ga:NH_2$ and $(C_2H_5)_3Ga:NH_2$ ions corresponding to 130/132 (Figure 3b) and 172/174 amu (Figure 6b), respectively. Note that these features can be generated in the QMS either by ionization of the associated parent molecule or by ionization/fragmentation of a molecule of higher mass. Although not unique, the simplest explanation as to the production of these features originates in the photolysis of NH_3 to make NH_2. It is known that NH_3 molecules resonantly absorb 193 nm photons (absorption cross section $\sim 1 \times 10^{-17}$ cm^{-2})[20] and predissociate in this electronic state on a sub-picosecond time scale to produce NH_2 radicals.[21,] A subsequent addition reaction of NH_2 with $(CH_3)_3Ga$ or $(C_2H_5)_3Ga$ in the presence of a third body will form $(CH_3)_3Ga:NH_2$ or $(C_2H_5)_3Ga:NH_2$, respectively.

Laser power dependence studies can yield insight into the origins of these individual mass spectral features. Figure 8 presents results for the case of TEGa reacting with NH_3. Here, measurements show a power regime over which the $(C_2H_5)_3Ga:NH_2^+$ ion signal saturates. One expects such saturation to occur given the aforementioned large absorption cross section for the X → A transition of ammonia.[20] Note that if the photolysis region saturates, then NH_2 production is power independent thereby suggesting that its subsequent chemistry would not be enhanced by increasing the photolysis power.

If one equates the saturation behavior for the $(C_2H_5)_3Ga:NH_2^+$ ion signal with the NH_3 absorption cross section, the photolysis power density or photon intensity in the reaction region of the nozzle can be calculated. According to the rate equation for a two-level system with no mechanism to return to the ground state, the ground-state population $N(t)$ at any time t is given by

$$N(t) = N_0\, e^{-\sigma I t} \tag{1}$$

where N_0 is the initial ground-state population, σ is the absorption cross section, and I is the photolysis photon intensity. Assuming both a quantum yield close to unity for NH_2 formation[22] and a rapid rate of formation (i.e., a picosecond time scale),[21] the number of radicals formed $N^*(t)$ is given by

$$N^*(t) = N_0 - N(t) = N_0(1 - e^{-\sigma I t}) \tag{2}$$

and the relative amount of new product formed can be expressed as

$$N^*(t)/N_0 = 1 - e^{-\sigma I t} \tag{3}$$

The photon intensity I in the reaction region can be estimated by fitting the experimental data for the $(C_2H_5)_3Ga:NH_2$ ion signal with the ammonia saturation curve ($\sigma_{NH3} \sim 1 \times 10^{-17}$ cm^{-2}) using this equation, as shown in Figure 8. Although photon intensities can be roughly determined experimentally through direct measurement of the laser beam, this procedure constitutes a route by which a reference laser power regime can be established. Note that, for the purposes of calculation, the laser pulse is taken to be temporally square ($t = 23 \times 10^{-9}$ s).

Having established a basis for comparison, one can look at the power dependence behavior of other precursor molecules as well as other ion features. Figure 8 shows the expected TEGa saturation curve ($\sigma_{TEGa} = 9 \times 10^{-18}$ cm^{-2})[23] as well as data for the $(C_2H_5)_3Ga_2(NH_2)_2$ ion signal at mass 257 amu. Clearly, the laser power dependence behavior for this ion feature containing two Ga atoms is much different than that for the saturated $(C_2H_5)_3Ga:NH_2$ ion signal. Although photolysis of TEGa with subsequent reaction is a likely starting point for ultimate generation of $(C_2H_5)_3Ga_2(NH_2)_2^+$, the similarity of the NH_3 and TEGa absorption cross sections makes such a distinction difficult in this case. In the case of TMGa, however, Figure 9 demonstrates that when TMGa is used as the metalorganic precursor, the power dependence behavior for the digallium species, $(CH_3)_3Ga_2NH^+$, shifts accordingly with the change in absorption cross section of TMGa ($\sigma_{TMGa} = 2 \times 10^{-17}$ cm^{-2} at 193 nm).[23] Compared with the presumably NH_3-based feature, $(CH_3)_3Ga:NH_2^+$, the power dependence rise is steeper

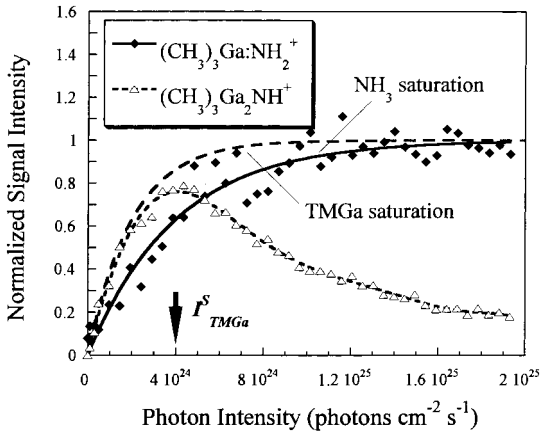

Figure 9. Normalized signal intensity of ion mass 130 amu, $(CH_3)_3$-Ga:NH_2, and ion mass 200 amu, $(CH_3)_3Ga_2NH$, as a function of photon intensity. The photon intensity is calculated by fitting $(CH_3)_3Ga{:}NH_2^+$ experimental data with eq 3 with ammonia absorption cross-section ($\sim 1 \times 10^{-17}$ cm^{-2}).

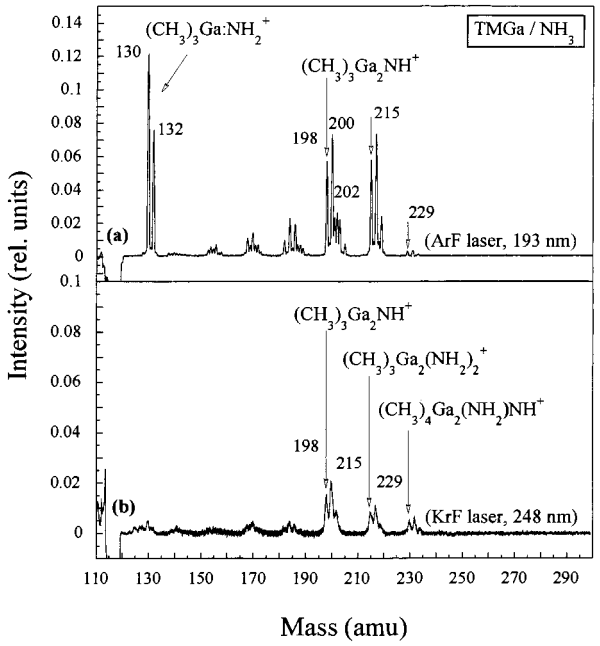

Figure 10. Mass spectra taken as a result of TMGa/NH_3 photolysis at two different wavelengths: (a) 193 nm and (b) 248 nm.

thereby reflecting the larger absorption cross section for TMGa. As shown in Figure 9, the signal reaches a maximum and then turns over, just as in the case for the $(C_2H_5)_3Ga_2(NH_2)_2$ ion. In contrast, the analogous NH_3-based feature, $(CH_3)_3Ga{:}NH_2^+$, simply saturates as expected if the initial step in its formation is the photolysis of NH_3.

Figure 10 provides additional evidence for a dual pathway mechanism for the formation of the peaks arising from the photoassisted reactivity of TMGa with NH_3. To produce Figure 10a, 193 nm radiation was used, while Figure 10b came about from 248 nm photolysis. The striking difference is that the relative intensity of the signal attributed to the $(CH_3)_3Ga{:}NH_2^+$ ion has diminished considerably upon going from 193 to 248 nm radiation. Since the absorption cross section for NH_3 becomes vanishingly small at 248 nm,[20] while the TMGa absorption cross section still persists,[23] it is not surprising that the primary feature arising from NH_3 photolysis also drops greatly in *relative* intensity. Note that all features have decreased in absolute intensity owing to the decrease in

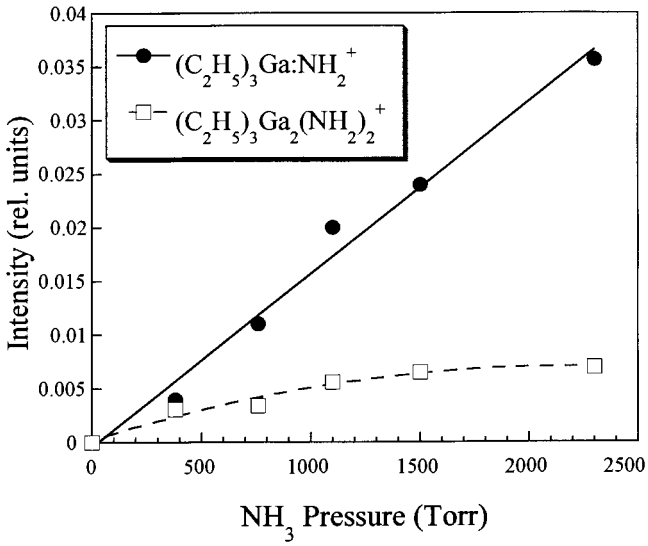

Figure 11. Intensity of ion mass 172 amu, $(C_2H_5)_3Ga{:}NH_2$, and ion mass 257 amu, $(C_2H_5)_3Ga_2(NH_2)_2$, as a function of ammonia pressure.

absorption cross section for both NH_3 and TMGa. However, the relative changes in intensity clearly confirm the photolytic origins of the 130 and 198 amu peaks as derived from Figure 9.

To explain the power dependence behavior for the digallium ion species shown in Figures 8 and 9, the initial step is most likely the 193 nm photolysis of TMGa or TEGa to simply cleave an ethyl or methyl group or perhaps generate CH_2 or C_2H_4 via α- or β-hydrogen elimination.[24−26] The internally excited gallium-containing photoproducts then subsequently undergo single or multiple reactions that lead eventually to the observed signal. However, the increase, saturation, and subsequent decrease of the ion signals of interest suggest that a second photolysis event is occurring. In this case, it is likely that either the parent molecule is absorbing a second photon, or a reactive, gallium-containing photoproduct is absorbing a photon. The result in either case is a "turning off" of the pathway that ultimately leads to the ion feature being observed. It should also be noted that the photon intensity where the $(CH_3)_3Ga_2$-NH and $(C_2H_5)_3Ga_2(NH_2)_2$ ion signals reach their maximum values (I^s_x) is inversely proportional to the absorption cross sections for TEGa and TMGa, i.e., $I^s_{TEGa}/I^s_{TMGa} \approx \sigma_{TMGa}/\sigma_{TEGa} \approx 2.0$. This fact may be coincidental, but it also suggests that perhaps the second step in the photolysis process is similar in each case. Finally, although we have not addressed it explicitly, reactions initiated through photon absorption by the $(CH_3)_3Ga{:}NH_3$ and $(C_2H_5)_3Ga{:}NH_3$ adducts themselves may play a role in the observed reactive chemistry. At present, we do not know enough about the absorption properties nor the concentrations of these species to adequately gauge their involvement.

D. Pressure Effects. In Figure 11, the effects of NH_3 pressure on the signals for masses 172 and 257 amu of Figure 6b are presented. Clearly, the $(C_2H_5)_3Ga{:}NH_2^+$ feature has a significant dependence on NH_3 pressure that is approximately linear. Such a dependence is consistent with a feature that has its origins in NH_3 photolysis, since doubling the pressure of the ammonia, for example, will double the intensity of the $(C_2H_5)_3Ga{:}NH_2^+$ signal. On the other hand, the relative insensitivity of the $(C_2H_5)_3Ga_2(NH_2)_2^+$ ion signal to NH_3 pressure means that all one needs is a sufficient amount of NH_3 present to maximize the signal with respect to NH_3. TEGa number density then becomes the limiting factor for generation

of the $(C_2H_5)_3Ga_2(NH_2)_2^+$ ion feature. In each case, the observations are consistent with the proposed initial photolysis pathways.

IV. Summary

Results for the formation of GaN-containing species in constrained expansions have been presented. Pulsed laser photolysis and a dual pulsed expansion assembly have been combined to explore the early stages of photoassisted growth. The method is not limited to GaN but can be applied to a variety of systems. Power and wavelength dependence studies allow one to identify the photolytic origins of individual ion features. Eventually, it may be possible to influence the deposition characteristics related to macroscopic film growth in an understandable fashion by altering the photolysis conditions as well as the composition of the gas mixture. While the current system is limited to studying only masses up to 300 amu, the experimental apparatus is being upgraded to explore masses up to 2000 amu.

Acknowledgment. Financial support from the Department of Energy, the State of Louisiana via the Louisiana Education Quality Support Fund, and the National Science Foundation is very much appreciated. An equipment donation from AT&T/Lucent is also gratefully noted.

References and Notes

(1) Ponce, F. A., Dupuis, R. D., Nakamura, S., Edmond, J. A., Ed. *Gallium Nitride and Related Materials;* Materials Research Society Symposium Proceedings 325; Materials Research Society: Pittsburgh, 1996.

(2) Ponce, F. A., Moustakas, T. D., Akasaki, I., Monemar, B. A., Ed. *III−V Nitrides;* Materials Research Society Symposium Proceedings 449; Materials Research Society: Pittsburgh, 1997.

(3) Abernathy, C. R., Amano, H., Zopler, J. C., Ed. *Gallium Nitride and Related Materials II;* Materials Research Society Symposium Proceedings 468; Materials Research Society: Pittsburgh, 1997.

(4) Dove, J. E.; Nip, U. S. *Can. J. Chem.* **1979**, *57*, 689.

(5) Jacko, M. G.; Price, S. J. V. *Can. J. Chem.* **1963**, *41*, 1560.

(6) Yashida, M.; Watanabe, H.; Vesugi, F. *J. Electrochem. Soc.* **1985**, *132*, 677.

(7) Riechert, H.; Averbeck, R.; Graber, A.; Schienle, M.; Strauss, U.; Tews, H. *Mater. Res. Soc. Symp. Proc.* **1997**, *449*, 149.

(8) Powers, D. E.; Hopkins, J. B.; Smalley, R. E. *J. Phys. Chem.* **1981**, *85*, 2711.

(9) O′Brien, S. C.; Liu, Y.; Zhang, Q.; Heath, J. R.; Tittel, F. K.; Curl, R. F.; Smalley, R. E. *J. Chem. Phys.* **1986**, *84*, 4074.

(10) Chaiken, J.; Casey, M. J.; Villarica, M. *J. Phys. Chem.* **1992**, *96*, 3183.

(11) Demchuk, A.; Porter, J.; Beuscher, A.; Dilkey, A.; Koplitz, B. *Chem. Phys. Lett.* **1998**, *283*, 231.

(12) Coates, G. E. *J. Chem. Soc.* **1951**, 2003.

(13) Andrews, J. E.; Littlejohn, M. A. *J. Electrohem. Soc.* **1975**, *122*, 1273.

(14) Zaouk, A.; Salvetat, E.; Sakaya, J.; Maury, F.; Constant, G. *J. Cryst. Growth* **1981**, *55*, 135.

(15) Moss, R. H. *J. Cryst. Growth* **1984**, *68*, 78.

(16) Almond, M. J.; Jenkins, C. E.; Rice, D. A. *J. Organomet. Chem.* **1992**, *439*, 251.

(17) Almond, M. J.; Drew, M. G. B.; Jenkins, C. E.; Rice, D. A. *J. Chem. Soc., Dalton Trans.* **1992**, *1*, 5.

(18) Thon, A.; Kuech, T. F. *Mater. Res. Soc. Symp. Proc.* **1996**, *395*, 97.

(19) Lide, D. R., Ed., *CRC Handbook of Chemistry and Physics*, 71st ed.; CRC Press, Inc.: Boston, 1990−1991.

(20) Okabe, H. *Photochemistry of Small Molecules*; Wiley-Interscience: New York, 1978; pp 269−272.

(21) Chung, Y. C.; Ziegler, L. D. *J. Chem. Phys.* **1988**, *89*, 4692.

(22) Ashfold, M. N. R.; Bennett, C. L.; Dixon, R. N. *Chem. Phys.* **1985**, *93*, 293.

(23) McCrary, V. R.; Donelley, V. M. *J. Cryst. Growth* **1987**, *84*, 253.

(24) Mitchell, S. A.; Hackett, P. A.; Rayner, D. M.; Humphries, M. R. *J. Chem. Phys.* **1985**, *83*, 5028.

(25) Brum, J. L.; Tong, P.; Koplitz, B. *Appl. Phys. Lett.* **1990**, *56*, 695.

(26) Beuerman, T.; Stuke, M. *Appl. Phys. B* **1989**, *49*, 145.